FISEVIER

Contents lists available at ScienceDirect

Applied Catalysis B: Environmental

journal homepage: www.elsevier.com/locate/apcatb



Toward concurrent organics removal and potential hydrogen production in wastewater treatment: Photoelectrochemical decolorization of methylene blue over hematite electrode in the presence of Mn(II)



TsingHai Wang^{a,*}, Chih-Ang Lin^b, Su Xu^b, Chu-Fang Wang^b, Chiu-Wen Chen^c, Cheng-Di Dong^c, C.P. Huang^{d,**}

- ^a Department of Chemical Engineering and Materials Sciences, Yuan Zu University, Zhongli, Taiwan
- ^b Department of Biomedical Engineering and Environmental Sciences, National Tsing Hua University, Hsinchu, Taiwan
- ^c Department of Marine Environmental Engineering, National Kaohsiung University of Science and Technology, Kaohsiung, Taiwan
- ^d Department of Civil and Environmental Engineering, University of Delaware, Newark, DE, USA

ARTICLE INFO

Keywords: Photoelectrochemical Decolorization Hydrogen production Sustainability Wastewater treatment

ABSTRACT

A sustainable system capable of simultaneous removal of organic contaminants and hydrogen generation in wastewater treatment operation was studied using hematite electrode in the presence of Mn(II), PEC-Mn(II), as a proof of concept. The photoelectrochemical (PEC) system exhibited methylene blue (MB) decolorization threefold faster than that of photo-Fenton processes and yielded comparable photocurrent density to relative to the control system, i.e., PEC water splitting in the absence of MB at otherwise identical operation conditions. Furthermore, the advantages of PEC-Mn(II) system were no H_2O_2 addition, hydrogen production potential, and ease in Mn(II) separation via the formation of MnO_2 precipitates during wastewater treatment operations. The PEC-Mn(II) process is a promising and sustainable approach toward wastewater treatment with the capability of concurrent photochemical energy generation. Moreover, the PEC-Mn(II) process can be an emerging energy-from-wastewater alternative in addition to other systems such as microbial fuel cell and anaerobic digestion.

1. Introduction

Photoelectrochemical (PEC) water splitting is an emerging technology capable of harvesting sunlight with the generation of lowcarbon-footprint energy, such as hydrogen, and curtailing globe warming problems due to CO2 emission. Hematite is an attractive photocatalyst because of its material abundance, chemical stability over a wide pH range, and favorable band gap structure capable of absorbing a wide spectrum of sunlight [1,2]. Large recombination loss due to low conductivity and consequently small carrier diffusion length and sluggish water oxidation kinetics, however, hinders the wide application of heterogensous photocatalysis [1,2]. A feasible approach to reduce the recombination loss is to effectively separate photogenerated electrons/ holes by, for example, applying a bias potential to drive electrons flow from the photoanode to a cathode [3] or introducing hole scavengers such as methanol or hydrogen peroxide to mediate hole accumulation at the catalyst/electrolyte interface [4]. In the latter case, methanol and hydrogen peroxide are oxidized by the holes, leading to a larger photocurrent density resulted from lowering recombination loss. The above observation has prompted us to hypothesize that once organic contaminants are oxidized by direct reaction with holes, a process similar to the addition of hole scavengers, there will emerge a new approach to conventional wastewater treatment system, which is capable of simultaneous organic degradation and hydrogen production in lieu of processes such as microbial fuel cells [5] and anaerobic digestion [6].

There have been experimentally demonstrated a series of photo-assisted electrochemical methods including photoelectron-Fenton, photoelectrocatalysis, solar photoelectrocatalysis, and solar photoelectron-Fenton, that exhibit high organics degradation efficiency in wastewater treatment [7]. Mechanism involved in photoassisted electrochemical system is strongly dependent on the production of reactive oxygen species (ROSs) such as 'OH, O_2^- , HO_2^+ , and H_2O_2 under incident light irradiation. Subsequent interactions between ROSs and the electrolytic system and/or quick photolysis of intermediates are mainly responsible for the high organics removal efficiency of photoassisted electrochemical methods, which can be described by reactions, Eq. (1)

^{*} Corresponding author at: Department of Chemical Engineering and Materials Science, Yuan Ze University, Zhongli, 320, Taiwan.

^{**} Corresponding author at: Department of Civil & Environmental Engineering, University of Delaware, Newark, DE 19716, USA. E-mail addresses: thwang@saturn.yzu.edu.tw (T. Wang), huang@udel.edu (C.P. Huang).

to Eq. (6), exemplified by hematite [7]:

$$Fe_2O_3 + h\nu \rightarrow e_{CB}^- + h_{VB}^+$$
 (1)

$$h_{VB}^{+} + H_2 O \rightarrow \bullet OH + H^{+}$$
 (2)

$$e_{CR}^- + O_2(ads) \rightarrow O_2^{\bullet -}$$
 (3)

$$O_2^{\bullet-} + H^+ \to HO_2^{\bullet}$$
 (4)

$$2HO_2^{\bullet} \rightarrow H_2O_2 + O_2$$
 (5)

$$H_2O_2 + O_2^{\bullet-} \rightarrow \bullet OH + OH^- + O_2$$
 (6)

where e_{CB}^- is the photoexcited electron in the conduction band and h_{VB}^+ is the hole remains in the valence band of the photocatalyst.

In the solar photoelectron-Fenton system of hematite/ Fe^{3+} photocatalyst, the high decolorization yield is attributed to the high efficiency in 'OH production from photolytic reactions, Eq. (7) and Eq. (8), and Fenton's reaction, Eq. (9) [8]. As 'OH generation is crucial to the system, it is thus not surprising that the decolorization efficiency increases with initial Fe^{3+} concentration and electrolysis time [9].

$$Fe(OH)^{2+} + h\nu \rightarrow Fe^{2+} + \bullet OH$$
 (7)

$$H_2O_2 + h\nu \rightarrow 2 \bullet OH$$
 (8)

$$Fe^{2+} + H_2O_2 \rightarrow Fe^{3+} + \bullet OH + OH^-$$
 (9)

In response to strong demands for sustainable wastewater treatment systems, efforts have been made to study the photoassisted electrochemical process. In fact, there are several successful cases using similar PEC based system for environmental applications reported in the literature. For example, the addition of chloride greatly enhanced contaminants degradation by the formation of chlorine radical ('Cl) [10,11] and reactive ClO₃ and ClO₄ oxidants [12]. In this case, preferential hydrogen evolution or ROS production was simply achieved by proper selection of cathode materials [13-15]. Formation of byproducts such as chlorate, perchlorate, chlorinated, and brominated organics would compromise the quality of the treated effluent [16]. Addition of H₂O₂ would further increase the 'OH production in a PEC system [17]. In the above cases, minimizing byproduct production could be attained by appropriately arranging the operation time [18,19] and working pH window [20]. By using a multi-junction semiconductor anode and a stainless steel cathode paired configuration, Hoffmann et al. reported that oxygen reduction reaction and hydrogen evolution would be suppressed to a certain degree in the presence of chloride and free chlorine, respectively [21,22]. Importantly, the authors also demonstrated that the treatment system could be fully driven by the electricity produced from a solar panel [23]. The presence of trace bromide was favored contaminant degradation as a result of formation of reactive bromate oxidant [24]. In this study, we proposed a PEC-based system, with certain degree of expansion, for the decolorization of methylene blue (MB) as model contaminant over hematite electrode in the presence of Mn(II) species. This is a system where simultaneous PEC hydrogen evolution at cathode and PEC MB decolorization over hematite anode could be achieved. Our results show that this system exhibits a MB decolorization rate threefold faster than that of simple photocatalysis. The present PEC-Mn(II) system has several advantages such as no H2O2 addition, easy separation of Mn(II) through the formation of MnO₂ precipitates, and potential hydrogen production during wastewater treatment. This PEC-Mn(II) system can be a promising sustainable wastewater treatment strategy; one that is capable of energy generation over current microbial fuel cells [5] and anaerobic digestion alternatives [6].

2. Materials and methods

2.1. Preparation of hematite electrodes

All chemicals used were of ACS grade (Sigma-Aldrich) and used as received. Detail preparation of hematite electrodes has been reported in our previous studies [25,26], which comprised of a low-temperature treatment for hematite phase development and a rapid high-temperature treatment for Sn diffusion, from FTO substrate, to hematite to increase the conductivity [3]. Briefly, the hematite electrodes (2 cm \times 1 cm, supported on fluorine doped tin oxide (FTO) substrates) were synthesized by hydrothermal reaction at 120 °C for 4 h in 0.1 M Fe (NO₃)₃ and 1.0 M NaNO₃ at pH 1.2. The as-obtained FeOOH precursor electrodes were then treated in two-step heating, 500 °C for 1 h followed by 750 °C for 10 min, at a heating rate of 10 °C-min $^{-1}$. Thirty hematite electrodes were prepared and those displayed a photocurrent of 0.60 \pm 0.15 mA/cm 2 at + 1.1 $V_{\rm RHE}$ were selected for further experiments.

2.2. MB decolorization

All experiments were conducted in triplicate in a home-made, undivided quartz glass cell (300 mL) equipped with three-electrodes, hematite working electrode (1 cm × 1 cm effective working area), platinum plate counter electrode (1 cm x 1 cm), and saturated calomel reference electrode (SCE), connected to a CHI 608E electrochemical workstation at pH = 2.5 and room temperature. Note that in this open, undivided system (without any sealing), both water oxidation (at anode) and water reduction (at cathode) simultaneously took place in the same reactor. This configuration made the measurement of hydrogen production yield at cathode challenging. Attentions were thus specifically on observing the variations in photocurrent as an alternative, since high photocurrent means more electrons are available, at cathode, for hydrogen evolution. The electrolyte was, unless otherwise mentioned, NaHCO3 (1.0 M), MB (10 mg/L or 0.03 mM), and 1.0 mM Mn(II) (ICP-MS standard solution, 1000 mg/L, Merck). The MB concentration was determined at the absorbance wavelength of 660 nm using a UV-vis spectrometer (Varian-Cary 50, Agilent). Blank experiment was conducted by direct illumination of the MB solution (without either Mn(II) nor hematite electrode) using simulated sunlight (AM 1.5 G, 100 mW/cm²). The control experiment of MB adsorption by hematite electrode was performed in dark and electrocatalysis (or electro-Fenton) was conducted under the same conditions as described above while a constant current of 0.2 mA was applied (operated in chronopotentiometric mode). Photocatalysis, in photo-Fenton mode, with/ without Mn(II), was carried out under simulated sunlight illumination on the front side of the electrochemical cell, without applied current. The PEC decolorization experiment was performed in chronopotentiometric mode (0.2 mA), with/without Mn(II) in the electrolyte unless otherwise mentioned. The dissolved oxygen concentration was determined using the MW600 standard portable dissolved oxygen meter (Milwaukee, USA) for the following systems: i) control (with hematite electrode only), ii) in the presence of Mn(II) (hematite electrode + 1.0 mM Mn(II), and iii) in the presence of both Mn(II) and MB (hematite electrode + 1.0 mM Mn(II) + 10 mg/L MB). The total organic carbon concentration in the PEC decolorization system, in the presence of 1.0 mM Mn(II), was also determined using TOC-L TOC Analyzer (Shimadzu, Japan) (Tables 1 and 2).

2.3. Characterization

Scanning electron microscopy (SEM, JSM700 F, JEOL) and high resolution transmission electron microscopy (HRTEM, EOL JEM-2100 HRTEM) equipped with energy dispersive X-ray analysis (EDX) were used to characterize the deposited MnO₂ precipitates. X-ray photoelectron spectrometer (XPS, PHI Quantera SXM/Auger) was utilized to

Table 1 Rate constants of MB decolorization at different conditions according to the pseudo first-order kinetics model ($lnC_0/C_1 = k_1t$) [25].

Conditions	Rate constant (k ₁ , min ⁻¹)	R ²	Description
Blank	5.37×10^{-4}	0.963	Irradiated by simulated sunlight only
Ad	5.37×10^{-4}	0.963	Adsorption in the dark
EC	5.37×10^{-4}	0.963	Electrocatalysis
PC w/o Mn(II)	1.24×10^{-2}	0.958	Photocatalysis without Mn(II)
PC	1.73×10^{-2}	0.966	Photocatalysis with Mn(II)
PEC w/o Mn(II)	1.83×10^{-2}	0.941	Photoelectrocatalysis without Mn (II)
PEC	5.96×10^{-2}	0.989	Photoelectrocatalysis with Mn(II)

 $\label{eq:table 2} \mbox{Rate constant of MB decolorization as a function of Mn(II) concentration according to the pseudo first-order kinetics model (lnC_0/C_t = k_1t) [25].}$

[Mn(II)] (mM)	Rate constant (k_1, \min^{-1})	R^2
0	1.84×10^{-2}	0.940
0.10	4.21×10^{-2}	0.998
0.25	6.72×10^{-2}	0.971
0.50	6.82×10^{-2}	0.956
0.75	6.75×10^{-2}	0.973
1.00	5.96×10^{-2}	0.989

identify the oxidation state of Mn species on hematite surface after illumination. In addition, linear sweep voltammetry was also conducted in chopping mode, from $-0.5\ V_{SCE}$ to $1.0\ V_{SCE}$, for the above three systems to evaluate the PEC water splitting efficiency. Potential, measured with reference to saturated calomel reference electrode (SCE), V_{SCE} , were converted to that of reversible hydrogen electrode, V_{RHE} , according to the following equation: $V_{RHE}=V_{SCE}+0.242+0.059 pH$.

3. Results and discussion

3.1. Kinetics of MB decolorization at different conditions

Fig. 1 shows the kinetics of MB decolorization at various experimental conditions. Apparently, no significant MB decolorization (< 3%) was observed under direct simulated sunlight illumination (photolysis), by adsorption (ad), and by electrocatalytic (specifically, the electrochemically catalytic) decolorization (EC) (Note that all three sets of data overlap each other as shown in Fig. 1). Results indicated clearly that MB decomposition by simulated sunlight irradiation alone was negligible. Strong electrostatic repulsion between the positively charged hematite surface and cationic MB under acidic condition resulted in low decolorization efficiency by adsorption [27].

By contrast, the low electrocatalytic decolorization was likely a result of low direct charge transfer (direct oxidation) as well as low hydroxyl radical (ROS) supply in the system (no light irradiation) [28]. It is worthy of mention that although H_2O_2 can be produced via the two-electron reduction of dissolved O_2 at 0.68 V_{RHE} (Eq. (10)) [8,29] we speculate that this was not the case as most electrons are anticipated being driven to the cathode already for hydrogen production $(2H^+ + 2e^- \rightarrow H_2, V_{RHE} = 0)$. This speculation was made based on recent studies on the dynamics of photogenerated charge carriers in hematite and their impact upon the efficiency of water photoelectrolysis [3,30,31]. By using the techniques such as transient absorption spectroscopy, transient photocurrent spectroscopy, and electrochemical impedance spectroscopy, Le Formal and co-workers concluded that the rate constant for water oxidation was ca. 0.5 s^{-1} , while that of the back electron recombination was roughly 2–200 times faster (in the 1–100

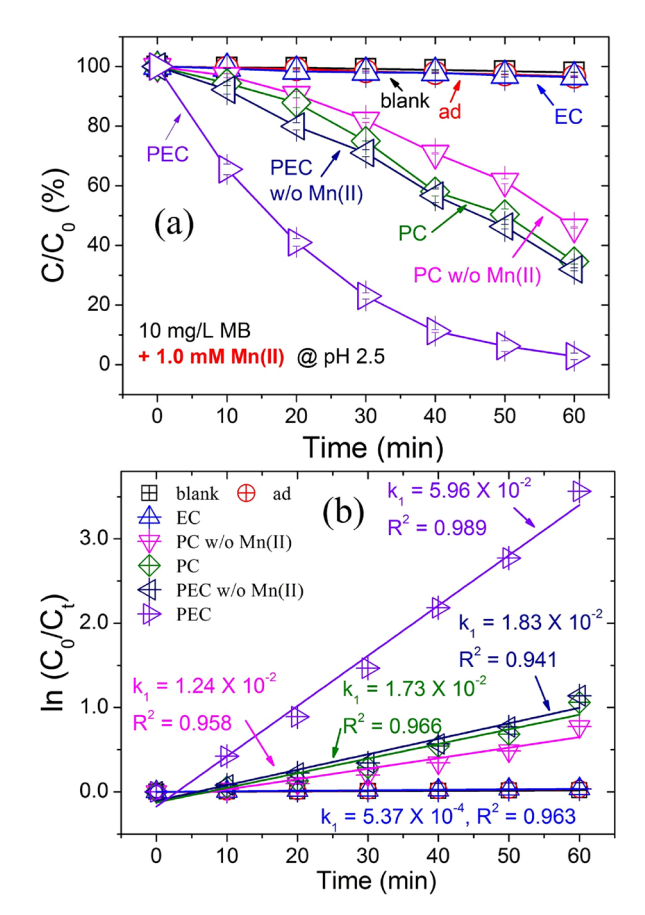


Fig. 1. (a) The kinetics of MB decolorization at different conditions; (b) fitting results of data shown in (a) by the linearized pseudo first-order kinetics model $(\ln C_0/C_t = k_1 t)$ [25], where C_0 and C_t refer to the MB concentration at the initial and time t, respectively; Note: ad = adsorption; EC = electrocatalysis; PC = photocatalysis; PEC = photoelectrocatalysis.

s⁻¹) [31]. Importantly, the recombination process could be increased to 10 ms to 1 s time scale depending upon the applied bias [31]. Applied potential-dependent lifetime of photogenerated charge carriers was also reported by Barroso and Durrant, who concluded that applied bias could effectively separate photogenerated electrons and holes by at least three orders of magnitude with respect to the time required for e_{CB} transport to the FTO [3]. A rate law analysis of PEC methanol oxidation further indicated that the reaction rate was strongly sensitive to the density of surface holes [30]. This again supports our speculation that the availability of surface holes is key in ROS production. In addition, low 'OH production during electrocatalysis was also caused by the limited availability of Fe(II). This is because, as mentioned above, the applied bias transfers majority of electrons to the cathode that diminishes the replenish of Fe(II), which is derived from the reduction of Fe(III). The combination of low availability of H₂O₂ and Fe(II) consequently led to low 'OH yield compared to conventional Fenton's reaction (Eq. (9)) and thus low decolorization efficiency. This observation, again, supports the notion that the majority of generated carriers are likely to participate in water splitting instead of ROSs formation at the cathode. Indeed, results of PEC methanol oxidation clearly implicated that the second-order kinetics of methanol oxidation was directly related to the density of surface holes on both hematite and titania [30]. The rate-limiting step of PEC oxidation is essentially controlled by the charge transfer from the catalysts to the adsorbed molecules (methanol from the literature and MB in this study). Based on our results and previous literature studies [3,30,31], we proposed that the availability of surface holes is key to affecting the efficiency of MB decolorization. On the other hand, Mn(II) is likely to catalyze the kinetics of water

oxidation instead of ROSs generation [25], which accounts for the low MB decolorization observed in Fig. 1.

$$O_2(g) + 2H^+ + 2e^- \rightarrow H_2O_2$$
 (10)

Fig. 1b shows the linearized pseudo-first order rate plots. It is noted that the rate constant for the PEC- Mn(II) system was almost twice that of the PEC only system (Fig. 1b). The significant increase in MB decolorization can be simply attributed to the high efficiency in concomitant OH generation via photolytic reaction (Eq. (7)) and Fenton's reaction (Eq. (9)) [8,32]. Without hydrogen peroxide addition, H₂O₂ formation must be derived from the interaction between dissolved oxygen and adsorbed water on the surface of hematite electrode and the photoexcited electrons/holes through reactions (Eqs. (1)-(5)) [7,33]. On the other hand, Mn(II) effectively catalyzes reaction (Eq. (6)) [34,35], leading to approximately 40% faster decolorization (per the determined k₁ value) compared to the system without Mn(II), presumably due to higher 'OH production yield. Furthermore, it is likely that reaction between Mn(II) and Fe(III) occurred spontaneously, that reduces and regenerates Fe(III) to Fe(II), which further reacts with hydrogen peroxide to form hydroxyl radicals according to following reaction [36]:

$$Fe^{3+} + e^{-} \rightarrow Fe^{2+}; E^{0} = 0.771 V_{RHE}$$
 (11)

$$Mn^{3+} + e^{-} \rightarrow Mn^{2+}; E^{0} = -1.5 V_{RHE}$$
 (12)

Combination of Eq. (11) and Eq. (12) yields

$$Fe^{3+} + Mn^{2+} \rightarrow Mn^{3+} + Fe^{2+}$$
; $E^o = 2.271 V_{RHE} > 0$

Positive E^o (2.271 V_{RHE}) indicated spontaneous reduction of Fe(III) to Fe(II) by Mn(II).

It is worthy of mention that a large population of e^-_{CB}/h^+_{VB} in the electrocatalysis (EC) system was generated as a result of the passing constant current (0.2 mA) throughout the experiment. However, results of MB decolorization clearly suggested that EC was less effective in MB decolorization than the photocatalytic system (PC). This again indicated that MB decolorization was more favorable by ROSs attack (i.e., the PC system) than direct oxidization by h^+_{VB} (i.e., the EC system). Furthermore, the protonated MB possesses an appropriate HOMO-LUMO energy gap structure that can effectively absorb visible light relative to its neutral species [37].

$$MB + hv \rightarrow MB^* \tag{13}$$

This means that the photoexcited MB species (referred as MB* hereafter) readily produces MB-bearing radical ('MB) and other secondary ROSs by interacting with Fenton reagents, i.e., the spiked Mn(II) and the reduced Fe(II) at the surface of hematite electrode.

In the case of PEC decolorization without Mn(II), its decolorization efficiency was comparable to that of photocatalysis (based on the comparable k1 constant, Fig. 1b). However, we highly speculate that the mechanism involved in these two systems is distinctly different. This is because the applied bias suppressed recombination loss and enabled more photogenerated carriers to participate in ROS formation. Furthermore, in the PEC system, the majority of photogenerated e_{CR} was transported to the cathode for hydrogen generation. This indicates that the formation of $O_2^{\bullet-}$ via reaction (Eq. (3)) as well as other ROSs generation via reaction (Eqs. (4)–(6)) was highly unlikely. Importantly, decolorization through direct MB oxidation by h_{VB} was negligible as no significant decolorization was observed by electrocatalysis (EC) even in the presence of Mn(II) catalyst. Note that both EC and PEC decolorization without Mn(II) were operated under the identical chronopotentiometric mode (0.2 mA), therefore, the amount of h_{VB} generation should be equal in these two systems. Based on this consideration, the observed efficiency between the two systems should be closely related to 'OH yield per reaction (Eq. (2)). Consistent with above discussions, direct MB oxidization by h_{VB} in the former (EC) case is less favorable and light irradiation in the PEC system is important to hydroxyl radical production. Specifically, the high decolorization rate by

PEC without Mn(II) over that by EC should be highly related to ROSs generation from the interaction between MB* species and the electrolyte. The same explanation also holds for the high decolorization by photocatalysis (photo-Fenton) as sunlight irradiation is essential to MB* generation (Eq. (13)). We therefore argue that the high decolorization by PEC without Mn(II) is the combination of efficient utilization of h_{VB}^{+} through the suppressed recombination loss and its subsequent interactions with MB* species to produce secondary ROSs.

Interestingly, spiking Mn(II) further enhances the PEC decolorization by approximately threefold in comparison with the system without Mn(II) (Fig. 1b). Obviously, the interaction between MB* species and Mn(II) species, instead of the number of catalytic sites at the hematite surface in both cases, is highly speculated important to MB decolorization [38]. It also accounts for the low MB decolorization yield by electrocatalysis as no MB* is available for ROSs generation. Based on the above observations, we hypothesize that ROS production from charge transfer between Mn(II) and MB* is mainly responsible for the high degree of decolorization in the PEC-Mn(II) system. Results of our previous studies revealed that a greater capacitance, suggested by the area under the CV scan, in dark scan than under illumination, was achieved by Mn(II) in situ passivation of the surface state of hematite electrodes [25]. This inferred that Mn(IV), from Mn(II) oxidation by h⁺_{VB} on the hematite surface, would be reduced to Mn(II) immediately by further transferring h_{VB}^+ to water, which accelerated water oxidation (homogeneous catalysis). We speculate that this catalytic behavior occurs in the PEC decolorization as well. That is, in addition to $\ensuremath{h_{VB}^{+}}$ transfer from Mn(IV) to MB*, h_{VB}^+ would concomitantly be transferred to water. Importantly, in this case, more \boldsymbol{e}_{CB}^{-} is available for hydrogen evolution at the cathode because of suppressed recombination loss. This phenomenon is exactly applicable to the development of a sustainable system that simultaneously removes hazardous organics from wastewater and generates hydrogen energy.

3.2. Effect of Mn(II) addition on MB decolorization

In order to verify the above hypothesis that charge transfer between Mn(VI) and MB* species is the rate-determining step in MB decolorization, a series of PEC decolorization experiments were conducted by varying the Mn(II) concentration. As shown in Fig. 2a, enhanced MB decolorization was noted as long as Mn(II) was present and amongst all conditions, adding 0.25-0.50 mM of Mn(II) led to the highest degree of MB decolorization. By fitting the data with the pseudo first-order kinetics equation (Fig. 2b), it was noted that the decolorization rate constant (k₁) increased proportionally with Mn(II) concentration to 0.25 mM, remained constant in the Mn(II) concentration range of 0.25 to 0.75 mM, and then slightly decreased as Mn(II) concentration was further increased to 1.0 mM. Given that all systems were subjected to the same intensity of simulated sunlight irradiation, the amount of photoexcited MB* species could be reasonably constant (reaching dynamically equilibrium). Accordingly, the rate constant increasing with Mn(II) concentration in the low [Mn(II)] region (< 0.25 mM) could be simply attributed to more Mn(II) available for the charge transfer reaction between Mn(IV) and MB*, which consequently enhanced decolorization. When [Mn(II)] exceeds 0.25 mM, the Mn(VI) species overwhelmed MB*, and the availability of MB* became the limiting step in MB decolorization. This speculation is supported by the observation that MB decolorization was insensitive to Mn(II) concentration in the [Mn(II)] > 0.25 mM region (Fig. 2b). Once again, the role of photoexcitation of MB species was important in MB decolorization as no significant MB decolorization was observed by electrocatalysis (EC in Fig. 1a) [39,40]. To support our argument that charge transfer between Mn(II) species and MB* was the rate-determining step in MB decolorization in addition to ROSs generation. The effect of Mn(II) concentration on decolorization can be described by the following reac-

First, adsorption of Mn(II) onto the catalyst surface (S refer to the

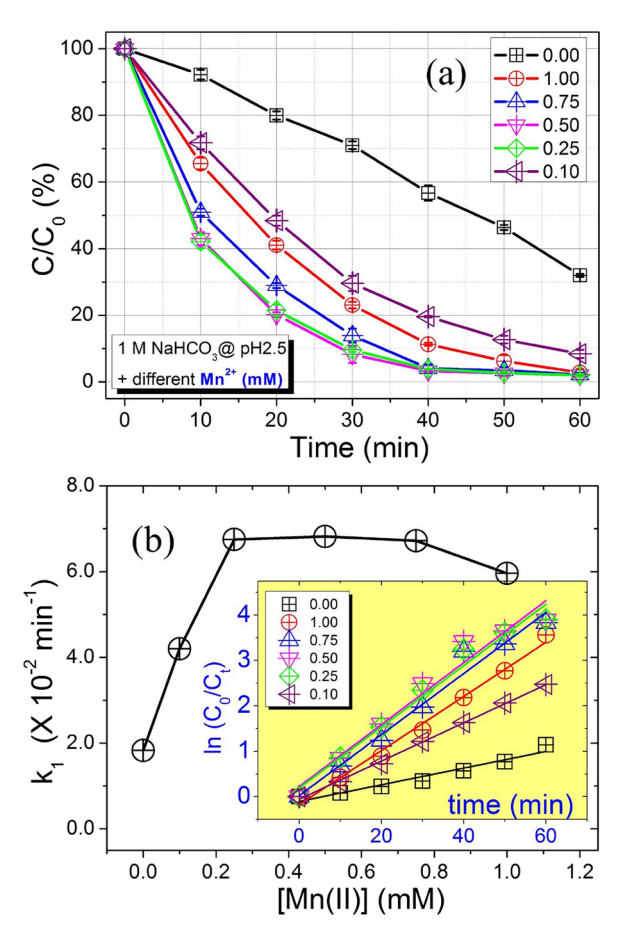


Fig. 2. (a) Effect of Mn(II) concentration on MB decolorization; (b) fitting results of data shown in (a) by the linearized pseudo first-order kinetics model.

surface of hematite) take place rapidly to reach equilibrium:

$$S + Mn(II) \leftrightarrow S - Mn(II); K = \frac{[S - Mn(II)]}{[S][Mn(II)]}$$
(14)

Given that the total surface site, S_T , is the sum of free plus occupied sites, one has:

$$S_{T} = [S] + [S-Mn(II)]$$

$$(15)$$

Combining Eq. (14) and Eq. (15) and solve for [S], one has:

$$[S] = \frac{S_{T}}{(1 + K[Mn(II)])}$$
(16)

Substituting Eq. (16) in Eq. (15), yields:

$$[S-Mn(II)] = \frac{KS_{T}[Mn(II)]}{(1 + K[Mn(II)])}$$
(17)

As mentioned above, photolysis of MB forms MB* and reaches dynamically equilibrium as soon as being irradiated, i.e.,

$$MB + hv \rightarrow MB^* \tag{13}$$

Assuming that the reaction between MB* and adsorbed Mn(II), S-Mn(II), species is the rate limiting step, i.e.,

S- Mn(II) + MB*
$$\rightarrow$$
 products; k2 (18)

From Eq. (18), the rate of MB degradation can be expressed as:

$$-\frac{d[MB^*]}{dt} = k_2[S-Mn(II)][MB]$$
 (19)

Substituting Eq. (17) in Eq. (19), one has:

$$-\frac{d[MB^*]}{dt} = k_2 \frac{KS_T[Mn(II)]}{(1 + K[Mn(II)])} [MB^*] = k_{obs}[MB^*]$$
 (20)

where

$$k_{obs} = \frac{k_2 K S_T [Mn(II)]}{(1 + K[Mn(II)])}$$
(21)

Eq. (20) is a Langmuir–Hinshelwood reaction kinetics. At low [Mn (II)], that is, K[Mn(II)] < 1; $k_{\rm obs}$ can be approximated as $k_2 K S_T [Mn(II)],$ which indicates that the rate constant, $k_{\rm obs}$, is proportional to Mn(II) as observed in Fig. 2b. By contrast, at high [Mn(II)], that is K[Mn(II)] > 1, $k_{\rm obs}$ can be approximated as $k_2 S_T$, which accounts for the observation in Fig. 2b that the rate constant, $k_{\rm obs}$, is constant when [Mn(II)] > 0.25 mM.

Solid evidence further supports the dual role of Mn(II) in dye decolorization and hydrogen production by observing the variation in applied bias in response to sustaining the constant 0.2 mA current throughout the decolorization experiment (Fig. 3a). In the PEC decolorization system, without Mn(II) (red line), applied bias rapidly increased from 0.80 $V_{\rm RHE}$ to 1.26 $V_{\rm RHE}$ in the first three minutes and then gradually reached a steady voltage of 1.42 $V_{\rm RHE}$ in 30 min. The steep increment can be realized by the rapid accumulation of h_{VB}^+ at the hematite/electrolyte interface that inevitably requires a greater applied bias to sustain the constant current. On the other hand, the relatively slow charge transfer between the water oxidation intermediates and MB* is insufficient to effectively suppress the recombination loss of h_{VB}^+/e_{CB}^- , which explains the gradual increment in the applied bias observed to sustain the constant current.

On the contrary, rapid oxidation of Mn(II) to Mn(IV) by h_{VB}^+ from hematite surface occurred in the PEC decolorization system (blue line), which effectively mediated h_{VB} accumulation, resulting in the less steep increment in applied bias in the first 10 min. Importantly, the steady applied bias of both PEC decolorization systems, with/without Mn(II) (1.40 V_{RHE} to 1.44 V_{RHE}), was rather close to the applied bias for PEC water splitting (black line, 1.42 V_{RHE}). The result supports above hypothesis and further implicates that MB decolorization concomitantly occurs with water splitting in the PEC system. We highly speculate that this phenomenon is attributed to the hydrogen evolution at cathode, where water is reduced by e_{CR}^- to molecular H_2 , and is unaffected by the oxidation conditions at anode. Indeed, as shown in Fig. 3b the dissolved oxygen (DO) content in all systems gradually increased until a relative degree of saturation was reached, meaning that oxygen evolution reaction did occur at the hematite anode surface. Importantly, the DO content rapidly increased upon Mn(II) addition, which substantially indicated the dual role of Mn(II) in concurrently MB decolorization and water splitting. It must be mentioned that the observed high water splitting potential is also resulted from the less reactive Mn(IV) in acidic than alkaline pH conditions due to the inherent instability of Mn(III) in acidic condition [41]. In addition to PEC water splitting, the complete MB decolorization in 60 min in the presence of 1.0 mM Mn(II) further indicated the efficiency of Mn(II) in catalyzing the heterogeneous photo-Fenton system [42]. Based on the above observations, Fig. 3c shows the proposed scheme accounting for the high PEC decolorization efficiency with Mn(II). Unlike other conventional advanced oxidation processes such as photoassisted electrochemical methods, our PEC-Mn (II) system brings further advances in effective utilization of the Mn(II)/ Mn(IV) redox shuttles for ROSs generation to accelerate MB decolorization while generates hydrogen at cathode by taking advantages of the suppressed recombination loss.

3.3. Separation of added Mn(II)

In addition to decolorization efficiency, success of the present PEC system is the effective removal of Mn(II) in post wastewater treatment. Apparently, Mn(II) was removed as $\text{MnO}_2(s)$ precipitates at the end of wastewater treatment. From SEM images, the surface morphology of

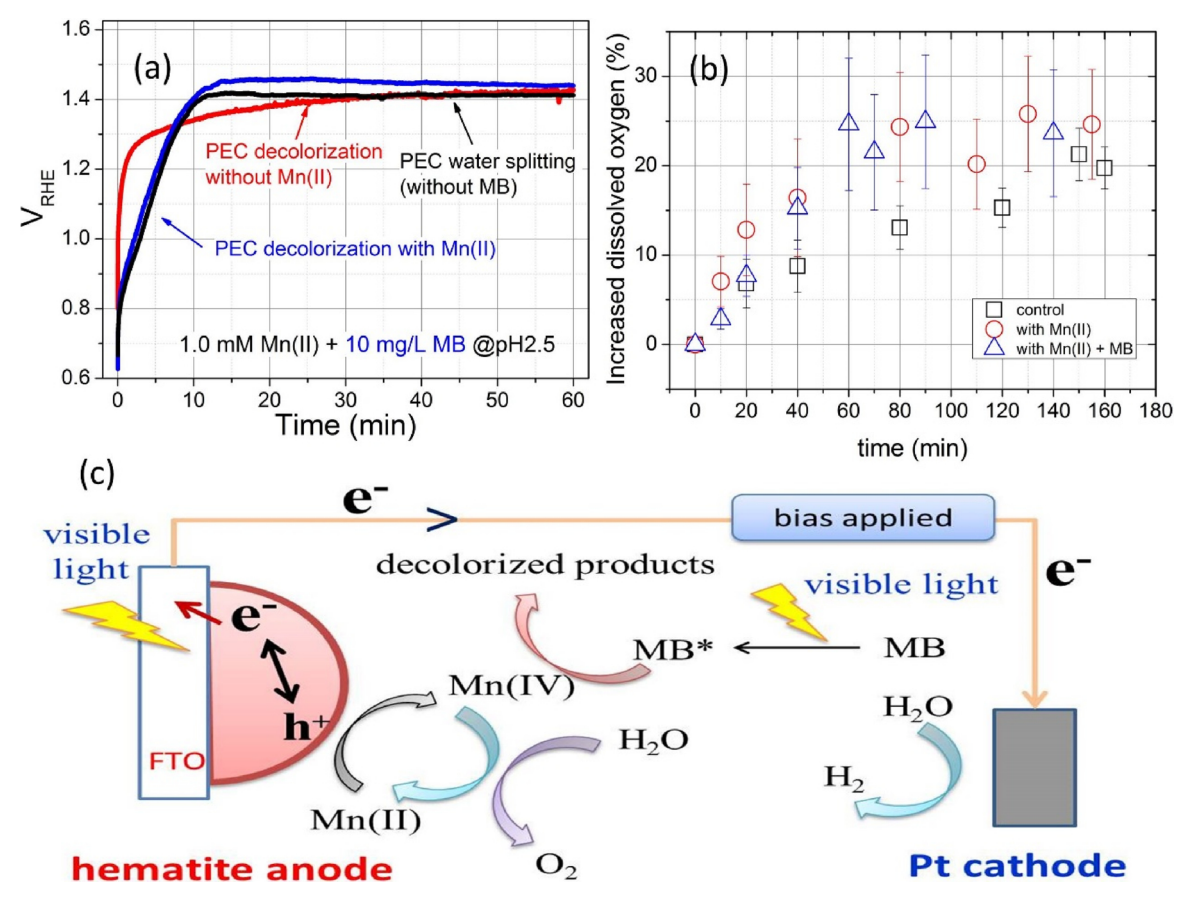


Fig. 3. (a) Corresponding voltage recorded in the PEC with/without spiking Mn(II) and the control systems operated under the chronopotentiometric mode (0.2 mA); (b) increment of dissolved oxygen in these systems; note that the data are presented in the increment percentage to minimize the fluctuations on the initial dissolved oxygen contents among these three systems; (c) proposed reaction routes for the high efficiency in PEC decolorization with Mn(II) additives.

hematite electrode was essentially composed of clusters of round hematite particles (Fig. 4a). At the end of PEC decolorization in the presence of Mn(II), the hematite surface was covered with flakes of MnO₂ precipitates (identified by SEM/EDX analyses) as shown in Fig. 4b. In fact, MnO₂ precipitates were found at the bottom of the reactor in all systems where Mn(II) was added (Fig. 4c), which clearly indicated that the spiked Mn(II) could be readily separated. The removal of Mn(II) in the form of MnO2(s) is exactly similar to that of the Fe electrocoagulation system where Fe(II) is removed in co-precipitation of lepidocrocite or hydrous ferric oxide [43]. Results of TEM/EDX (Fig. 4d and e) and XPS (Fig. 4f) showed clearly that the precipitates were amorphous MnO₂. Note that as shown in Fig. 3a, the system was rather stable in the course of one hour operation while MB decolorization was reached in 40 min (Fig. 1a). As a proof-of-concept presented in the present study, formation of MnO2 precipitates instead of photocorrosion of hematite anode would be a major process stability concern.

Question arises. Why Mn(II) precipitated as amorphous MnO_2 in this study but was present as Mn(II) on the hematite surface when it was *in situ* passivated surface states as we reported in our previous study [25]? Specifically, why Mn(III) was further oxidized to Mn(IV) and then was reduced to Mn(II) considering the thermodynamic instability of Mn (III) species? A possible explanation would be the formation of intermediate-stabilized Mn(IV) complexes. In the case of photocatalytic degradation of diethyl phthalate by biochar suspensions, it was demonstrated that the fully conjugated cyclic dione structure of biochar carbon matrix as well as its derivatives (such as dissolved organic matter) was capable of effectively stabilizing radicals through the resonance in the conjugated structure. This phenomenon is known as the persistent free radicals (PFRs), which is beneficial to the formation of other secondary ROSs [44]. In the ferric citrate system, PFRs can serve

as electron sink by donating electrons to ferric citrate, leading to fast Fe (II)/Fe(III) redox cycle [45], while the formation of either ${}^{\cdot}$ OH or $O_2^{\bullet-}$ is reported to be closely dependent on the band gap structure of the carbonaceous matrix [46]. Based on above literature studies, the degradation intermediate seems to be responsible for stabilizing MnO₂ precipitates. Results of total organic carbon (TOC) analyses indicated that despite a near complete MB decolorization, there was actually < 10% MB mineralized (Fig. 5a). Houas et al. [33] have indicated that MB degradation involves the formation of a series of small aromatic intermediates, which are capable of forming metal-ligand complexes [44-46]. We thus speculated that the degradation intermediates were responsible for stabilizing Mn(IV)-bearing intermediates. Formation of Mn(IV) complexes retarded their reduction to Mn(II), resulting in the higher steady applied bias observed at 0.04 $\ensuremath{V_{RHE}}$ compared to the steady applied bias of PEC water splitting (without MB, Fig. 3a), and hence the separation of Mn(II) could be achieved readily in this system.

3.4. Effect of PEC condition on photocurrent

In addition to the complete separation of Mn(II) added, the most significant feature of our present system is the potential of generating hydrogen energy in wastewater treatment. As shown in the inserted panel in Fig. 5b, results of the linear sweep voltammetry clearly suggested that the photocurrent of the control system (no MB and Mn(II) is present, black line) was about threefold higher than the photocurrent of the system without Mn(II) (red line). This implicated that at least two-third of photogenerated $h_{\rm VB}^+/e_{\rm CB}^-$ were annihilated by recombination loss when MB was present, which could be attributed to the slow interfacial charge transfer [47]. By contrast, spiking Mn(II) profoundly led to a photocurrent (blue line) comparable to that of the control system. This

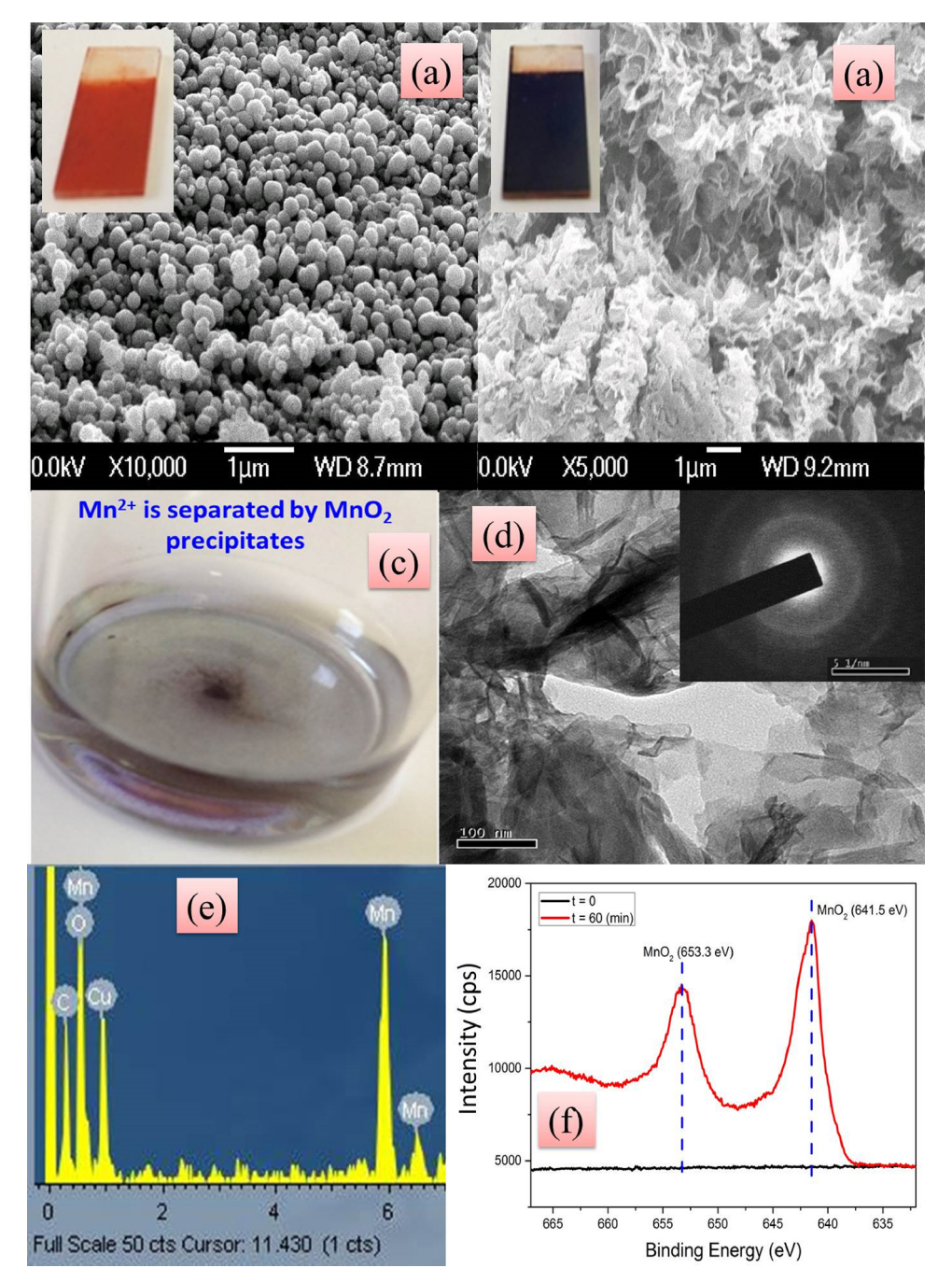


Fig. 4. SEM images of hematite electrode at (a) the beginning and (b) the end of PEC MB decolorization in the presence of $1.0 \, \text{mM}$ of Mn(II); (c) optical images of MnO₂ precipitates appearing at the bottom of reactor at the end of decolorization; (d) TEM image of the microstructure of MnO₂ precipitates collected from (c) and their selected area electron diffraction image, (e) element characterization by attached EDX analysis; and (f) identification of the oxidation state by XPS characterization.

suggested that the spiked Mn(II) functioned as an efficient Mn(II)/Mn (IV) redox shuttle that minimized the recombination of charge pairs [25,41]. Importantly, result further indicated that there was a comparable amount of $e_{\rm CB}^-$ available for cathodic hydrogen evolution while the complete MB decolorization occurred concurrently over the hematite anode. The result unambiguously suggested that the concomitant wastewater treatment and energy generation could indeed be achieved, which was exactly a sustainable approach developed in the present study. Similar concomitant wastewater treatment and hydrogen production system has been demonstrated using TiO₂-based PEC system [39,40], in which the amount of H_2 production is proven to increase proportionally with increasing current density. On the other hand, the

 O_2 generation is noted to be slightly lower than the expected stoichiometric water splitting (half of hydrogen generation) [39,40], meaning a fraction of h_{VB}^+ is indeed participating in 'OH generation. Both our results and those reported in the literature unambiguously suggest that efficient utilization of photogenerated h_{VB}^+/e_{CB}^- is critical to developing sustainable system capable of concomitant wastewater treatment and hydrogen production [47].

Another research topic deserving further exploration would be the fate of ROS and how MB is decolorized in our proposed PEC-Mn system. As discussion above, the involved reaction mechanism was complicate by several competing charge transfer steps, i.e., photogenerated electrons for cathodic hydrogen evolution and holes for anodic MB

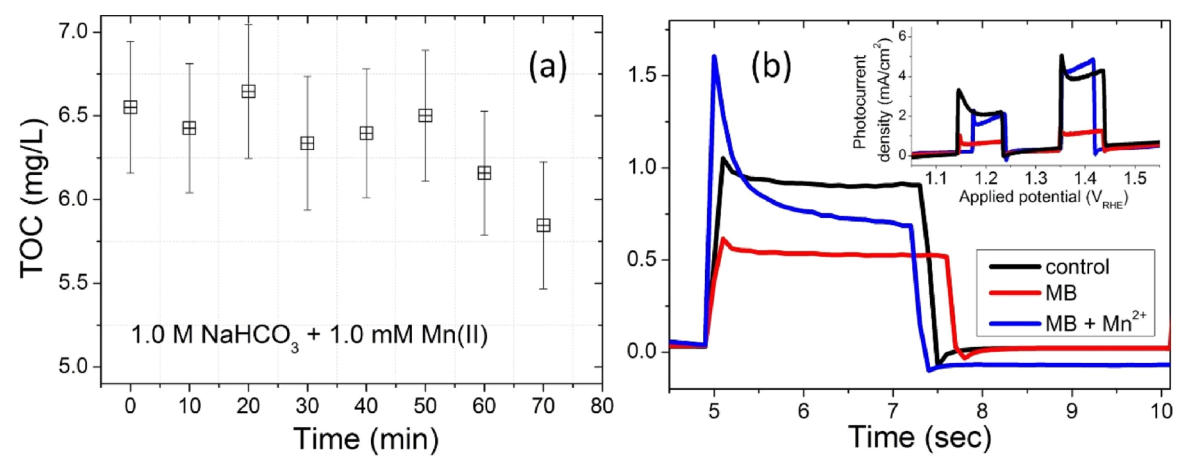


Fig. 5. (a) Variation of total organic carbon (TOC) in the PEC MB decolorization system with spiking Mn(II); (b) the i-t curve (current vs time) of the control system (no MB and Mn(II), black) and the PEC MB decolorization system w/o 0.5 mM Mn(II) additive (blue line and red line) recorded at applied 1.0 V_{RHE} in chopping mode. Insert: The linear sweep voltammetry scan of the three systems. (For interpretation of the references to colour in this figure legend, the reader is referred to the web version of this article).

decolorization. In this proof-of-concept study, we have proposed a reaction mechanism (Fig. 3c), essentially established based on the basis of experimental observations in different MB decolorization conditions, such as a PEC system with or without Mn(II) (Fig. 1a). Yet, the involved reaction kinetics was not fully understood. Utilization of ROS probes such as coumarin for 'OH [48], EDTA for hole scavenger [46], tetranitromethane of O₂⁻⁻ [32], as well as electron paramagnetic resonance (EPR) analysis of persistent free radicals trapped by DMPO [45] could be shed light on the reaction mechanisms. Furthermore, our PEC MB decolorization was conducted in an open, undivided cell where both water oxidation at anode and water reduction at cathode took place concurrently in the same reactor. This means that the measurement of hydrogen production yield and consequently the charge efficiency calculation is rather challenging. Separating anode and cathode halfreaction with an ion exchange membrane [40] would be necessary for gaining insights into the radical economy of the proposed PEC-Mn system.

To gain insight into the photocurrent behaviors in the three systems, the i–t curve (current vs time) was recorded by applying 1.0 $V_{\rm RHE}$ in chopping mode. It is noted that the area under the i–t curve (proportional to the amount of generated carriers) of the PEC MB decolorization system with/without Mn(II) addition (blue line and red line) were about 10% and 43%, respectively, which was lower than that of the control system (black line, Fig. 5b). A significant transient photocurrent in the PEC MB decolorization system with spiking Mn(II) (blue line) implied that there were additional one-third carriers not being annihilated by recombination loss, which were available for MB decolorization. Again, this confirmed the high efficiency of the spiked Mn(II) redox shuttle in minimizing the recombination of charge pairs [25,41].

3.5. Technology challenges and opportunities

Last but not the least, a sustainable system is never limited to the concurrent hydrogen acquisition in a wastewater treatment process. Any progress in the reduction of waste and energy consumption is a substantial step toward green wastewater treatment. In fact, by comparing our PEC system to that of others as reported in the literature, it becomes clear that there are still great challenges to be overcome before the deployment of PEC system in environmental applications. In general, efforts are specifically needed in three aspects, namely, improving charge carrier efficiency, wide working window, and system optimization. With respect to charge carrier efficiency improvement, a good example is the indirect cathodic and direct anodic generation of chlorine radical ('Cl) (in addition to 'OH production via Eq. (2)) [10].

Chlorine radical can selectively transform ammonia nitrogen to N_2 (79.9%) and NO_3^- (19.2%) [11]. Similarly, active chlorine (ClO_3^- and ClO_4^-) indirectly generated at cathode via dissolved chlorine gas (electrically reduced chloride at cathode) are reactive ROS too [12]. Selective yielding of active chlorine or hydrogen could be achieved by replacing platinum cathode with carbon, stainless steel [13,14], and Ni foam [15].

Efficient utilization of charge carrier is further closely related to the working window of a PEC-based wastewater treatment system [16]. The PEC phenol degradation over $BiVO_4$ anode and Cu_2O/CuO cathode has been demonstrated in a broad working pH range (4–7) [17]. Suppressing toxic byproduct production such as chlorate and perchlorate is another important issue of public health concern in wastewater treatment [16]. Terminating the PEC reaction after ammonium removal efficiently minimizes byproduct formation without compromising disinfection and nutrient removal [18]. This is because free chlorine radial is the principal oxidant in the system [19], and the presence of sulfate enhances the generation of undesired chlorate and perchlorate at both acidic and neutral pH [20].

Regarding system optimization, Hoffmann et al. have proposed a prototypical wastewater electrolysis cell consisting of a multi-junction semiconductor anode and a stainless steel cathode paired in a single compartment cell [21]. They have concluded that chloride reduces the electron consumption during O₂ reduction, while elevated levels of free chlorine significantly lowers the current efficiency for the hydrogen evolution reaction [22]. High COD and NH₄ removal can be achieved after 2 h with minimal energy consumption (370 kW h/kg COD and 383 kW h/kg NH₄) [22]. Importantly, the whole electrocalaytic system can be completely operated with solar-driven photovoltaic panels [23]. Sedlak et al., further indicate that the transformation rates for most contaminants increase in the presence of chloride and trace amounts of bromide [24]. However, increase in HCO₃ concentration often decreases the reactivity toward electron-poor contaminants and increase the reactivity for compounds with amine and phenolic moieties [24]. Accordingly, integration of a PEC system with an anaerobic biodegradation system to fractionate COD into proteins, carbohydrates, and carboxylates could benefit further efficiency enhancement [18]. Finally, better understanding the limitations of the PEC system, particularly in the aspect of the potential health risks by the byproduct, significantly determines the design and operation of a PEC-based treatment system [16].

4. Conclusion

We have demonstrated a sustainable system capable of concomitant organics removal and hydrogen generation by utilizing photoelectrochemically (PEC) decolorization of methylene blue (MB) over hematite electrode in the presence of Mn(II). In addition to achieving a threefold faster MB decolorization, there was approximately 90% photocurrent remained with respect to the PEC water splitting system (system without MB) for potential hydrogen evolution or ROS production at cathode. The presence of Mn(II) significantly decreased hole-electron recombination and improved the photooxidation of organic compounds. The PEC-Mn(II) system enabled the efficient use of photogenerated electrons for cathodic hydrogen generation. The present PEC-Mn(II) system provides a viable alternative to current processes such as microbial fuel cell and anaerobic digestion for energy extraction during wastewater treatment.

Acknowledgments

The authors wish to thank the Ministry of Science and Technology, Taiwan, for the support of this study by research grants: MOST 105-2113-M-007-022-MY2 and MOST 107-2113-M-007 -005 -MY2. Addition support was provided by US NSF IOA (1632899).

References

- O. Zandi, T.W. Hamann, The potential versus current state of water splitting with hematite, Phys. Chem. Chem. Phys. 17 (35) (2015) 22485–22503.
- [2] D. Kang, T.W. Kim, S. Kubota, A. Cardiel, H.G. Cha, K.-S. Choi, Electrochemical synthesis of photoelectrodes and catalysts for use in solar water splitting, Chem. Rev. 115 (23) (2015) 12839–12887.
- [3] M. Barroso, S.R. Pendlebury, A.J. Cowan, J.R. Durrant, Charge carrier trapping, recombination and transfer in hematite (α-Fe₂O₃) water splitting photoanodes, Chem. Sci. 4 (7) (2013) 2724–2734.
- [4] J.R. Swierk, T.E. Mallouk, Design and development of photoanodes for watersplitting dye-sensitized photoelectrochemical cells, Chem. Soc. Rev. 42 (6) (2013) 2357–2387.
- [5] B.E. Logan, B. Hamelers, R.A. Rozendal, U. Schrorder, J. Keller, S. Freguia, P. Aelterman, W. Verstraete, K. Rabaey, Microbial fuel cells: methodology and technology, Environ. Sci. Technol. 40 (17) (2006) 5181–5192.
- [6] L. Appels, J. Baeyens, J. Degreve, R. Dewil, Principles and potential of the anaerobic digestion of waste-activated sludge, Prog. Energy Combust. Sci. 34 (6) (2008) 755-781
- [7] E. Brillas, C.A. Martinez-Huitle, Decontamination of wastewaters containing synthetic organic dyes by electrochemical methods: an updated review, Appl. Catal. B 166 (2015) 603–643.
- [8] A.R. Khataee, B. Vahid, B. Behjati, M. Safarpour, Treatment of a dye solution using photoelectro-Fenton process on the cathode containing carbon nanotubes under recirculation mode: investigation of operational parameters and artificial neural network modeling, Environ. Progr. Sustain. Energy 32 (3) (2013) 557–563.
- [9] A.R. Khataee, M. Zarei, A.R. Khataee, Electrochemical treatment of dye solution by oxalate catalyzed photoelectro-Fenton process using a carbon nanotube-PTFE cathode: optimization by central composite design, Clean 39 (5) (2011) 482–490.
- [10] C. Kim, S. Kim, S.P. Hong, J. Lee, J. Yoon, Effect of doping level of colored TiO₂ nanotube arrays fabricated by electrochemical self-doping on electrochemical properties, Phys. Chem. Chem. Phys. 18 (21) (2016) 14370–14375.
- [11] Y.Z. Ji, J. Bai, J.H. Li, T. Luo, L. Qiao, Q.Y. Zeng, B.X. Zhou, Highly selective transformation of ammonia nitrogen to $\rm N_2$ based on a novel solar-driven photoelectrocatalytic-chlorine radical reactions system, Water Res. 125 (2017) 512–519.
- [12] S.L. He, Q. Huang, Y. Zhang, L.Z. Wang, Y.L. Nie, Investigation on direct and indirect electrochemical oxidation of ammonia over Ru – Ir/TiO₂ anode, Ind. Eng. Chem. Prod. Res. Dev. 54 (5) (2015) 1447–1451.
- [13] Z.G. Aguilar, E. Brillas, M. Salazar, J.L. Nava, I. Sires, Evidence of Fenton-like reaction with active chlorine during the electrocatalytic oxidation of acid Yellow 36 Azo dye with Ir-Sn-Sb oxide anode in the presence of iron ion, Appl. Catal. B. 206 (2017) 44–52
- [14] C.M. Dominguez, N. Oturan, A. Romero, A. Santos, M.A. Oturan, Lindane degradation by electrooxidation process: effect of electrode materials on oxidation and mineralization kinetics, Water Res. 135 (2018) 220–230.
- [15] Y. Zhang, J.H. Li, J. Bai, Z.X. Shen, L.S. Li, L.G. Xia, S. Chen, B.X. Zhou, Exhaustive conversion of inorganic nitrogen to nitrogen gas based on a photoelectro-chlorine cycle reaction and a highly selective nitrogen gas generation cathode, Environ. Sci. Technol. 52 (3) (2018) 1413–1420.
- [16] J. Radjenovic, D.L. Sedlak, Challenges and opportunities for electrochemical processes as next-generation technologies for the treatment of contaminated water, Environ. Sci. Technol. 49 (19) (2015) 11292–11302.
- [17] X. Li, S.S. Liu, D. Cao, R. Mao, X. Zhao, Synergetic activation of H₂O₂ by photogenerated electrons and cathodic Fenton reaction for enhanced self-driven

- photoelectrocatalytic degradation of organic pollutants, Appl. Catal. B 235
- [18] J.T. Jasper, Y. Yang, M.R. Hoffmann, Toxic byproduct formation during electrochemical treatment of latrine wastewater, Environ. Sci. Technol. 51 (21) (2017) 7111–7119.
- [19] C.M. Chung, S.W. Hong, K. Cho, M.R. Hoffmann, Degradation of organic compounds in wastewater matrix by electrochemically generated reactive chlorine species: kinetics and selectivity, Catal. Today 313 (2018) 189–195.
- [20] A. Farhat, J. Keller, S. Tait, J. Radjenovic, Assessment of the impact of chloride on the formation of chlorinated by-products in the presence and absence of electrochemically activated sulfate, Chem. Eng. J. 330 (2017) 1265–1271.
- [21] K. Cho, M.R. Hoffmann, Molecular hydrogen production from wastewater electrolysis cell with multi-junction BiOx/TiO₂ anode and stainless steel cathode: current and energy efficiency, Appl. Catal. B 202 (2017) 671–682.
- [22] Y. Yang, J. Shin, J.T. Jasper, M.R. Hoffmann, Multilayer heterojunction anodes for saline wastewater treatment: design strategies and reactive species generation mechanisms, Environ. Sci. Technol. 50 (16) (2016) 8780–8787.
- [23] K. Cho, Y. Qu, D. Kwon, H. Zhang, C.A. Cid, A. Aryanfar, M.R. Hoffmann, Effects of anodic potential and chloride ion on overall reactivity in electrochemical reactors designed for solar-powered wastewater treatment, Environ. Sci. Technol. 48 (4) (2014) 2377–2384.
- [24] J.M. Barazesh, C. Prasse, D.L. Sedlak, Electrochemical transformation of trace organic contaminants in the presence of halide and carbonate ions, Environ. Sci. Technol. 50 (18) (2016) 10143–10152.
- [25] T.H. Wang, Y.J. Cheng, Y.Y. Wu, C.A. Lin, C.C. Chiang, Y.K. Hsieh, C.F. Wang, C.P. Huang, Enhanced photoelectrochemical water splitting efficiency of hematite electrodes with aqueous metal ions as in situ homogenous surface passivation agents, Phys. Chem. Chem. Phys. 18 (42) (2016) 29300–29307.
- [26] T.H. Wang, H.T. Huang, Y.R. Cheng, M.C. Huang, Y.K. Hsieh, C.F. Wang, Understanding the role of phosphate in the enhanced photocatalytic performance of Co-Pi/hematite photoanodes prepared through an solution based synthesis route, RSC Adv. 6 (34) (2016) 28236–28247.
- [27] T.H. Wang, C.J. Hsieh, S.M. Lin, D.C. Wu, M.H. Li, S.P. Teng, Effect of alkyl properties and head groups of cationic surfactants on retention of cesium by oragnoclays, Environ. Sci. Technol. 44 (13) (2010) 5142–5147.
- [28] Z.G. Aguilar, E. Brillas, M. Salazar, J.L. Nava, I. Sires, Evidence of Fenton-like reaction with active chlorine during the electrocatalytic oxidation of acid yellow 36 azo dye with Ir-Sn-Sb oxide anode in the presence of iron ion, Appl. Catal. B 206 (2017) 44–52.
- [29] F.C. Moreira, R.A.R. Boaventura, E. Brillas, V.J.P. Vilar, Electrochemical advanced oxidation processes: a review on their application to synthetic and real wastewaters, Appl. Catal. B 202 (2017) 217–261.
- [30] C.A. Mesa, A. Kafizas, L. Francas, S.R. Pendlebury, E. Pastor, Y.M. Ma, F. Le Formal, M.T. Mayer, M. Gratzel, J.R. Durrant, Kinetics of photoelectrochemical oxidation of methanol on hematite photoanodes, J. Am. Chem. Soc. 139 (33) (2017) 11537–11543.
- [31] F. Le Formal, S.R. Pendlebury, M. Cornuz, S.D. Tilley, M. Graetzel, J.R. Durrant, Back electron-hole recombination in hematite photoanodes for water splitting, J. Am. Chem. Soc. 136 (6) (2014) 2564–2574.
- [32] Y.Y. Liu, W. Jin, Y.P. Zhao, G.S. Zhang, W. Zhang, Enhanced catalytic degradation of methylene blue by alpha-Fe2O3/graphene oxide via heterogeneous photo-fenton reactions, Appl. Catal. B 206 (2017) 642–652.
- [33] A. Houas, H. Lachheb, M. Ksibi, E. Elaloui, C. Guillard, J.M. Herrmann, Photocatalytic degradation pathway of methylene blue in water, Appl. Catal. B 31 (2) (2001) 145–157.
- [34] Y.F. Li, J.H. Sun, S.P. Sun, Comparison of metoprolol degradation by Fe-III-NTA modified fenton-like reaction in the absence and presence of manganese: efficiency and intermediates, Chem. Eng. J. 313 (2017) 769–776.
- [35] S. Li, G.S. Zhang, P. Wang, H.S. Zheng, Y.J. Zheng, Microwave-enhanced Mn-Fenton process for the removal of BPA in water, Chem. Eng. J. 294 (2016) 371–379.
- [36] P. Atkins, J. de Paula, Physical Chemistry, 8th edition, Oxford University Press, 2006.
- [37] K. Sarmah, S. Pratihar, Synthesis, characterization, and photocatalytic application of iron oxalate capped Fe, Fe-Cu, Fe-Co, and Fe-Mn oxide nanomaterial, ACS Sustain. Chem. Eng. 5 (1) (2017) 310–324.
- [38] M.B. Ahmed, J.L. Zhou, H.H. Ngo, W.S. Guo, M.A. Johir, K. Sornalingam, Single and competitive sorption properties and mechanism of functionalized biochar for removing sulfonamide antibiotics from water, Chem. Eng. J. 311 (2017) 348–358.
- [39] M.S. Koo, K. Cho, J. Yoon, W. Choi, Photoelectrochemical degradation of organic compounds coupled with molecular hydrogen generation using electrochromic TiO₂ nanotube arrays, Environ. Sci. Technol. 51 (11) (2017) 6590–6598.
- [40] Y.-P. Peng, H.L. Chen, C.P. Huang, The synergistic effect of photoelectrochemical (PEC) reactions exemplified by concurrent perfluorooctanoic acid (PFOA) degradationand hydrogen generation over carbon and nitrogen codoped TiO₂ nanotube arrays (C-N-TNTAs) photoelectrode, Appl. Catal. B 209 (2017) 437–446.
- [41] T. Takashima, K. Hashimoto, R. Nakamura, Mechanisms of pH-dependent activity for water oxidation to molecular oxygen by MnO₂ electrocatalyst, J. Am. Chem. Soc. 134 (3) (2012) 1519–1527.
- [42] Y. Zhou, B. Xiao, S.Q. Liu, Z.D. Meng, Z.G. Chen, C.Y. Zou, C.B. Liu, F. Chen, X. Zhou, Photo-Fenton degradation of ammonia via a manganese-iron double-active component catalyst of graphene-manganese ferrite under visible light, Chem. Eng. J. 283 (2016) 266–275.
- [43] C.M. van Genuchten, J. Pena, Mn(II) oxidation in Fenton and Fenton type systems: identification of reaction efficiency and reaction products, Environ. Sci. Technol. 51 (5) (2017) 2982–2991.
- [44] G.D. Fang, C. Liu, Y.J. Wang, D.D. Dionysiou, D.M. Zhou, Photogeneration of

- reactive oxygen species from biochar suspension for diethyl phthalate degradation,
- Appl. Catal. B 214 (2017) 34–45. [45] L.S. Luo, D. Wu, D.J. Dai, Z.Y. Yang, L.K. Chen, Q.B. Liu, J.C. He, Y.Y. Yao, Synergistic effects of persistent free radicals and visible radiation on peroxymonosulfate activation by ferric citrate for the decomposition of organic contaminants, Appl. Catal. B 205 (2017) 404-411.
- [46] I. Velo-Gala, J.J. López-Penalver, M. Sánchez-Polo, H. Rivera-Utrilla, Role of activated carbon surface chemistry in its photocatalytic activity and the generation of
- oxidant radicals under uv or solar radiation, Appl. Catal. B 207 (2017) 412-423. [47] H. Park, H.I. Kim, G.H. Moon, W. Choi, Photoinduced charge transfer processes in
- solar photocatalysis based on modified TiO2, Energy Environ. Sci. 9 (2) (2016) 411-433.
- [48] Y. Nakabayashi, M. Nishikawa, N. Saito, C. Terashima, A. Fujishima, Significance of hydroxyl radical in photoinduced oxygen evolution in water on monoclinic bismuth vanadate, J. Phys. Chem. C 121 (46) (2017) 25624-25631.